Dynamic Failure Localization in Spinal Specimens using Acoustic Emissions

Jay K. Shridharani, Allison L. Schmidt, Courtney A. Cox, Brian R. Bigler, Anna E. Knight, Cameron R. 'Dale' Bass

Abstract

Understanding the dynamic failure behavior of the spine is important in prevention of acute spinal injuries and chronic spinal pain. Traditional failure identification techniques are poor indicators of less severe injuries including incipient failure. One promising technique for sensitively assessing spinal injury is dynamic mapping of acoustic emissions. This technique allows detection of small failures in the spine, which are important for understanding spinal injuries at occupational exposure levels and for understanding the progression of catastrophic spinal injuries.

A whole cervical spine was excised and instrumented with a position sensor, two 6-axis load cells, and an array of acoustic sensors. Tap tests were performed to determine the feasibility of using localization algorithms in the spine. The specimen was loaded in compression with increasing displacements until the first acoustic emission was measured. Acoustic emissions were localized with a mean error of 3.63mm and 10.7mm in the tap tests. The failure was localized to the right lateral side of C4 which was 12.2mm from a failure in the osteophyte seen in micro-CT and an associated failure in the anterior longitudinal ligament. These failures occurred during the loading and would not have been detected using traditional force time history analysis. This technique provides improved understanding of failure in spinal biomechanics, especially for low-level incipient and repeated loading injuries potentially associated with pain.

Keywords Acoustic sensor, fracture, lumbar spine, cervical spine, failure

I. INTRODUCTION

Cervical and lumbar spinal injuries lead to debilitating pain and widespread morbidity [1-3], which cause large societal expenses [4]. Understanding the dynamic failure mechanisms in the spine can help prevent spinal injury and pain. Previous in vitro studies subject spinal specimens to large loads inducing gross bony fractures or ligamentous injuries [5-9]. In vivo, these injuries have severe long-term consequences and could require surgical intervention. However, chronic neck and back pain may be associated with smaller localized failures such as endplate disruption, trabecular fractures, partial ligamentous tearing or the subsequent healing processes following these injuries. Currently, the failure mechanics of these injuries are not well understood. To better research these injuries, a methodology is needed that can induce and detect these injuries.

Traditional in vitro testing techniques assess specimen failure using a drop in load bearing with increasing displacement [5,8,10,11] or a change in the stiffness between subsequent tests [9]. These changes in structural response occur as a result of gross failures in the vertebral bodies or ligaments and are usually verified using computed tomography (CT) in clinical scanners with a maximum resolution of 625um. Higher resolution is necessary to identify minor failures due to the small size of trabecular bone constituents, which are approximately 90-220um in thickness [12].

Advances in piezoelectric technology have led to the development of high frequency acoustic sensors that are sensitive to bony and ligamentous failures. These sensors can detect acoustic emissions (AE), which are acoustic excitations of the bone or other tissue following releases of strain energy from the formation of micro-cracks [13]. Acoustic sensors have been used to determine the timing of failure in biological materials [14,15]. Allsop

J. K. Shridharani is a PhD candidate in Biomedical Engineering at Duke University in Durham, NC, USA (tel: +1 919-660-8272, fax: +1 919-684-4488, jay.shridharani@duke.edu). A. L. Schmidt, C.A. Cox, B.R. Bigler are PhD candidates and A. E. Knight is an undergraduate student in Biomedical Engineering at Duke University in Durham, NC. C. R. 'Dale' Bass is an Associate Research Professor in Biomedical Engineering at Duke University in Durham, NC.

et. al. showed that small acoustic emissions occur in temporo-parietal bone during the loading and a larger acoustic emission at the peak force. Funk et. al. also observed this phenomena in the foot/ankle complex, but also showed small acoustic events in specimens with no apparent failure. Both studies showed the larger acoustic emission corresponded to the time of the large failure, but it is likely that the smaller acoustic events are due to micro-cracks that would potentially cause pain in vivo or may lead to further progressive injuries in repeated loading [16]. Funk et. al. was also able to determine if the calcaneus or the pilon fractured first by placing an acoustic sensor on each of these bones and determining which sensor signal corresponded to a drop in the peak force. Van Toen et al. measured the frequency response of acoustic emissions generated by failing vertebral bodies and ligamentum flavum specimens. They found that ligament failure produces statistically significantly lower frequency emissions (20kHz – 30kHz) than bony failure (30kHz – 115kHz) [17]. This information can be useful in post-processing analyses to determine what type of tissue has failed based on the acoustic response. However, these in vitro studies do not analyze the smaller amplitude acoustic emissions occurring during loading. These smaller acoustic emissions are likely indicative of minor injuries that may cause incipient injuries to the spine or cause spinal pain. Understanding these acoustic emissions can give insight into injury biomechanics of incipient fracture and the biomechanics of the spine including back pain.

Arrays of acoustic sensors have been used to localize micro-cracking in many different materials in civil and aerospace engineering [13,18-20] by using a difference in time of arrival method. However, these methods have not yet been applied to biological materials with complex speeds of sound and inhomogeneous/anisotropic constituents. Localizing injuries in biological specimens will improve our understanding of the failure mechanics in the human spine and provide insight into sub-catastrophic injuries and exposures that may underlie chronic pain. The focus of this study is to apply acoustic emission localization techniques in a cadaveric cervical spine model and validate the fracture location calculation using micro-CT imaging.

II. METHODS

In this study, an isolated human cervical spine was subjected to compressive loading in a servohydraulic materials testing machine. A whole cervical spine (basilar skull–T1) was excised from a 51-year-old unembalmed male cadaver in accordance with research protocol approved by the Duke University Institutional Review Board. A pre-test clinical CT scan at 625um resolution was acquired prior to testing to verify the specimen was free of mechanical damage and to provide a comparison to post-failure scans.

Specimen Preparation

Soft tissue including musculature, fat and skin was removed leaving the osteoligamentous structure intact. The mandible was disarticulated to allow access to the basilar skull. Wood screws were inserted into the basilar skull and the inferior endplate of T1, and wire was wrapped around the screws to provide a lattice for adhesion of the potting materials. To distribute stresses at the attachment sites, polymethylmethacrylate (PMMA) (Dentsply International; York, PA) was molded around the bone-screw-wire attachment points. Then, the specimen was potted in square aluminum cups using a fast-curing urethane casting resin (#891, Golden West Mfg., Inc., Grass Valley, CA 95945). Motion was preserved at both the atlanto-occipital joint and the C7-T1 joint. The specimen was then placed in a servohydraulic materials testing machine with the superior pot rigidly attached to the frame and the inferior pot rigidly attached to the piston. The specimen was positioned with the Frankfort plane horizontal, the occipital condyles 6.8^{o} anterior of T1 and the T1 vertebral body tilted anteriorly at 31^{o}. A diagram of the setup is shown in Figure 1.

Sensor Instrumentation

One 6-axis load cell was attached to the superior specimen pot and another on the inferior pot. A linear position sensor was attached to the piston to measure the displacement history. The displacement and load cell transducers were sampled at 100kHz using a National Instruments data acquisition card (Model PCI-6259, National Instruments, Austin, TX 78759). Eight locations on the vertebral bodies lateral to the anterior longitudinal ligament (ALL) were cleaned of soft tissue and periosteum to expose the bone. Four locations on C3, two on C4, one on C5 and one on C6 (Figure 1) were marked and the x, y and z coordinates were measured using a MicroScribe digitizer (Model 3Dx, Immersion Corporation, San Jose, CA 95131). The bone was then degreased using acetone and miniature acoustic sensors (Model S9225, Physical Acoustic Corporation, Princeton Junction, NJ 08550) were glued to the marked locations on the bone using cyanoacrylate adhesive. Acoustic sensors were conditioned using pre-amplifiers (Model 2/4/6, Physical Acoustic Corporation, Princeton

Junction, NJ 08550) with 20dB gain, powered using constant current power supplies, and simultaneously acquired at 2MHz (Model USB-6366, National Instruments, Austin, TX 78759) for 4 seconds with 5ms of pretrigger data.

Tap Tests

Before the compressive loading test, tap tests were conducted to determine the feasibility of the acoustic emission localization algorithm in a whole cervical spine. Two locations on the cervical spine – one on the anterior surface of C4 and the other on the anterior surface of C7 (Figure 1) – were marked, and their x, y and z coordinates were measured using a MicroScribe. A 4mm flat-ended punch was pressed against the marked location and an acoustic signal was generated by tapping the opposite end of the punch with a small metal hammer. Three repeated tests were performed at each location to calculate a mean and standard deviation of the error in the localization. The time of arrival at each of the acoustic sensors was calculated as the zero crossing immediately before the signal crossed a threshold defined as ±5 standard deviations of the noise in the pretrigger data.

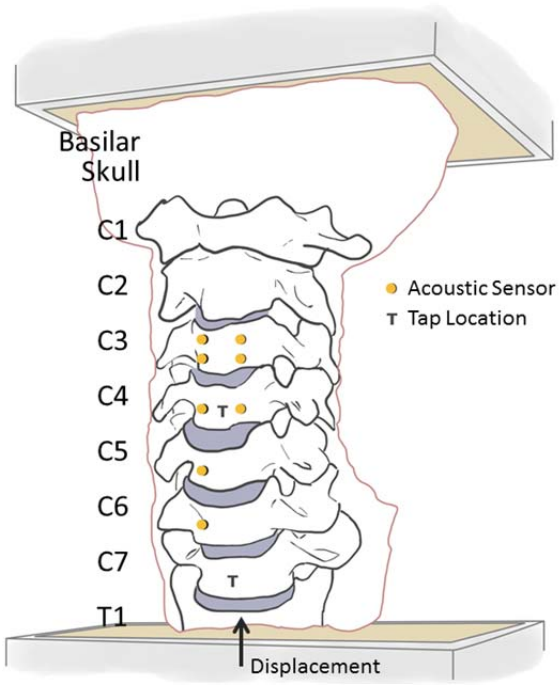

Figure 1. Oblique diagram of the specimen in the test apparatus showing the acoustic sensor and tap locations. The skull and T1 are embedded in the potting material. The upper fixture remains stationary, while the bottom is displaced.

Localization Algorithm

Localization was performed by using a time difference of arrival (TDOA) approach. The TDOA is the difference in the time of arrival of an acoustic emission at two sensors. The approach is developed around the basis that the TDOA is directly related to how much farther one sensor is from the acoustic emission source than the other sensor. By assuming a constant speed of sound, the Euclidian distance formulation is used to form the following system of equations:

$$\begin{aligned} c\,(t_2 - t_1) &= \sqrt{(x_s - x_2)^2 + (y_s - y_2)^2 + (z_s - z_2)^2} - \sqrt{(x_s - x_1)^2 + (y_s - y_1)^2 + (z_s - z_1)^2} \\ c\,(t_3 - t_1) &= \sqrt{(x_s - x_3)^2 + (y_s - y_3)^2 + (z_s - z_3)^2} - \sqrt{(x_s - x_1)^2 + (y_s - y_1)^2 + (z_s - z_1)^2} \\ c\,(t_4 - t_1) &= \sqrt{(x_s - x_4)^2 + (y_s - y_4)^2 + (z_s - z_4)^2} - \sqrt{(x_s - x_1)^2 + (y_s - y_1)^2 + (z_s - z_1)^2} \end{aligned} \quad (1)$$

where x_s, y_s and z_s are the x, y and z coordinates of the acoustic emission source; x_n, y_n and z_n are the x, y and z coordinates of the acoustic sensors; and t_n is the time of arrival of the acoustic emission at the sensor. The system of equations was solved using Matlab (R2013b, MathWorks, Natick, MA 01760) for x_s, y_s and z_s. The speed of sound was iterated upon until the solution converged. The error was then computed as the Euclidian distance between the computed and the measured location. All localizations on the inferior tap location were

performed using two sensors on C3, one on C6 and one on C5 while the localizations on the superior tap location were performed using the four sensors on C3.

Specimen Loading Protocol

After tap tests, the specimen was loaded by moving the piston upwards to apply a compressive ramp-hold load. To cause minor injuries, the peak displacement of the ramp was incremented until the first acoustic emission was observed. At this point, the specimen was considered to have failed and a post-test micro-CT was acquired (Nikon Metrology Inc., Model XTH 225 ST, Brighton, MI, 48116) at 90kVp, 290uAs, and 94.7um resolution to get radiographic imaging of the failure. The CT was reconstructed into a 3-D volume using Avizo (Version 8.0, FEI Visualization Sciences Group, Burlington, MA 01803) and the 2-D slices and 3-D volume were analyzed for failure.

III. RESULTS

The representative plot of the acoustic emissions in a tap test (Figure 2) shows the time history of the signal for the four sensors located on the C3 vertebral body for a tap on the C4 vertebral body. Each sensor shows a large voltage followed by an exponential decay of this signal. The largest voltage measured was 3.58V. As the sound arrives at each sensor, there is a much smaller voltage of almost 0.5V (Figure 3) from which the time of arrival was calculated. Localization of the acoustic emission source results in an error of 3.63 ± 0.6mm for the C4 tap location and 10.7 ± 2.3mm for the C7 tap location in terms of mean and standard deviation.

The time history of the force and acoustic signal (Figure 4) show low acoustic energy during the loading portion of the force trace followed by large acoustic emission where the specimen buckles in extension (115ms) and two additional large acoustic emissions after the peak force. Based on the acoustic signal in the sensor data, the time of arrival was computed for the acoustic emission as the specimen buckles to localize where the failure occurred. Performing this localization calculation using the four sensors located on the C3 vertebral body resulted in localizing the failure to the right lateral surface of the C4 vertebral body (Figure 5b).

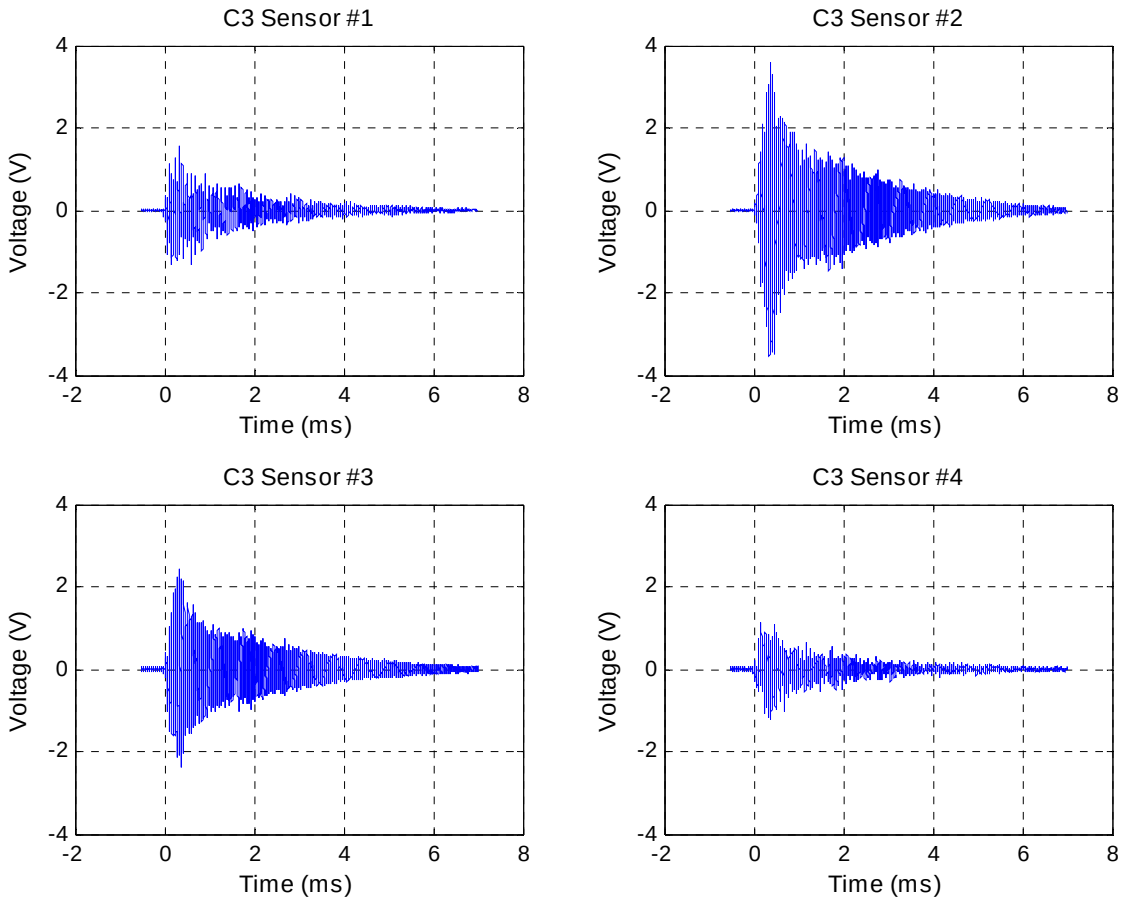

Figure 2. Representative time history of an acoustic emission measured by four sensors on the C3 vertebral body. The acoustic emission was generated by placing a metal punch against the surface of the ALL on C3 and lightly impacting the punch with a small metal hammer.

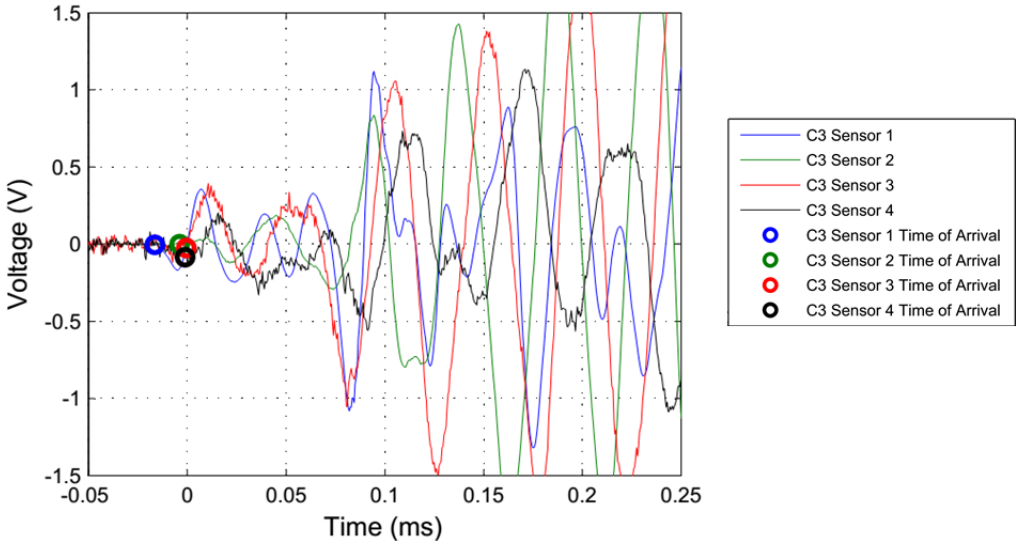

Figure 3. The initial time history of an acoustic emission measured by four sensors on the C3 vertebral body. The circles show the time of arrival calculated as the zero crossing immediately before the signal crosses a ±5 standard deviation threshold.

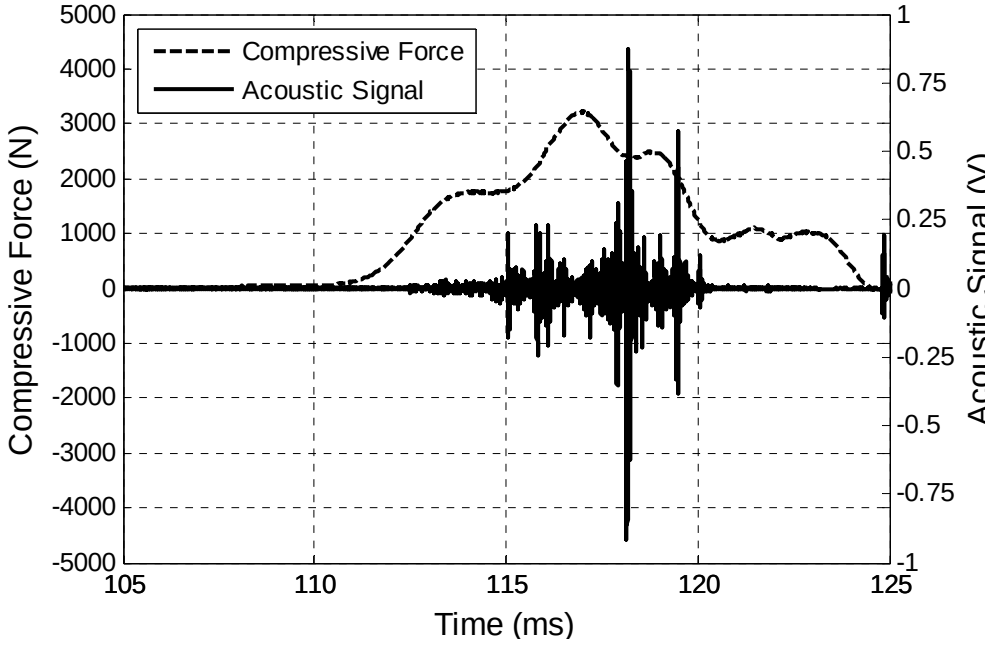

Figure 4. Example time history of the axial compressive force and the acoustic emission measured by one of the C3 sensors during the failure test show small acoustic signal during the loading, a larger acoustic signal during the buckling (115ms), and additional acoustic signal after the peak force.

The clinical and micro-CT reconstruction (Figure 5) provides a 3-D model of the bone before and after the test. In the pre-test scan (Figure 5a) there is an osteophyte bridging the anterior surfaces of the C4 and C5 vertebral bodies and there appears to be fusing of the C5-C6 joint space. The post-test scan (Figure 5b) clearly shows the osteophyte is dislodged from the C4 vertebral body and is only attached to C5. It also shows the calculated acoustic emission localization, which is 12.2mm from the osteophyte failure. No other failures were found in the cortical shell or trabeculae. The high-speed video confirms this fracture location and shows the osteophyte dislodging from the C4 vertebral body and possibly tearing the anterior longitudinal ligament. This

failure location was further confirmed in the post-test dissection (Figure 6), which also revealed tearing in the ALL at the same location.

The frequency response was computed for the sensor on the C4 vertebral body (Figure 7) adjusted for the nonlinearity in the sensor frequency response. The fundamental frequency of the acoustic emissions is wideband and has its maximum power at 24.5kHz. There are also two additional peaks at 66.7kHz and 79.7kHz. The spectrogram (Figure 8) provides an illustration how the power spectrum density of a 2000 point (1ms) Hamming window changes through the time history. Initially, there is low frequency content from 3.9kHz to 52.7kHz, which is followed by wider bands from 8.7kHz to 271.2kHz. The maximum power frequency enters the time domain at approximately 116 and 118ms, which corresponds to the failure seen in the high speed video.

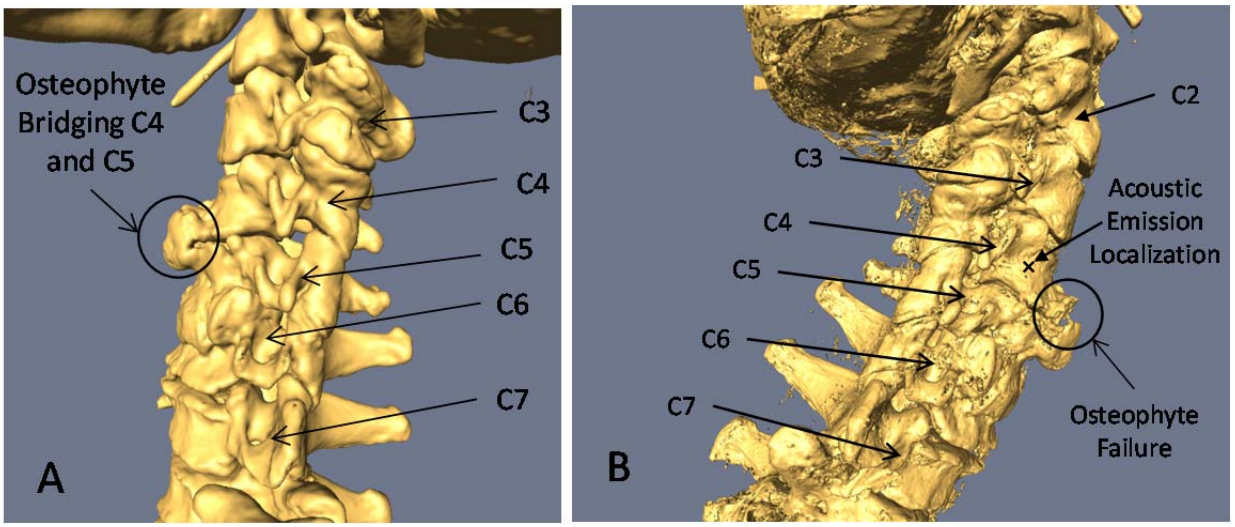

Figure 5. Pre-test clinical CT (a) showing an osteophyte bridging the anterior surfaces of the C4 and C5 vertebral bodies and (b) post-test micro-CT showing the osteophyte dislodged from the C4 vertebral body.

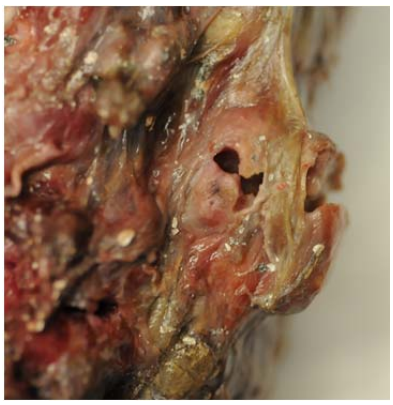

Figure 6. Post-test dissection showed a failure in the osteophyte bridging the C4 and C5 vertebral bodies as well as disruption in the ALL.

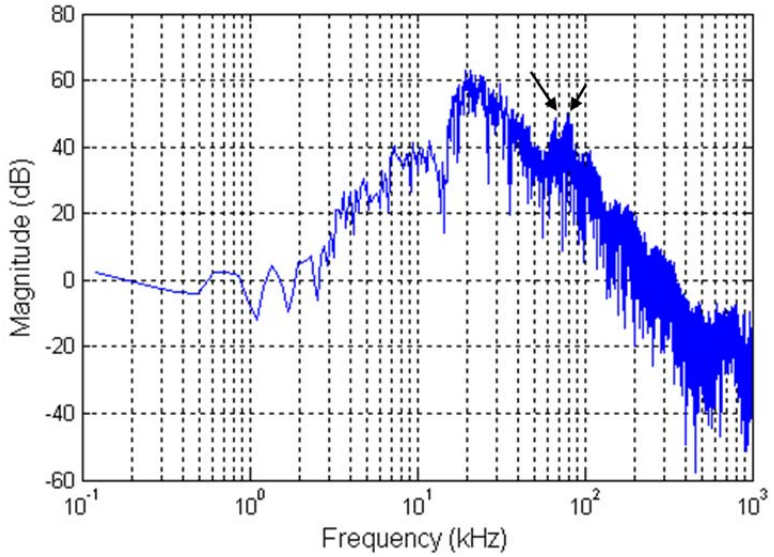

Figure 7. Frequency of the acoustic sensor on C4 during a failure test for a fracture in the osteophyte bridging the anterior surface of the C4 and C5 vertebral bodies. The maximum power occurs at 24.5kHz and there are two additional peaks at 66.7kHz and 79.7kHz, which is in the expected range for bony failure.

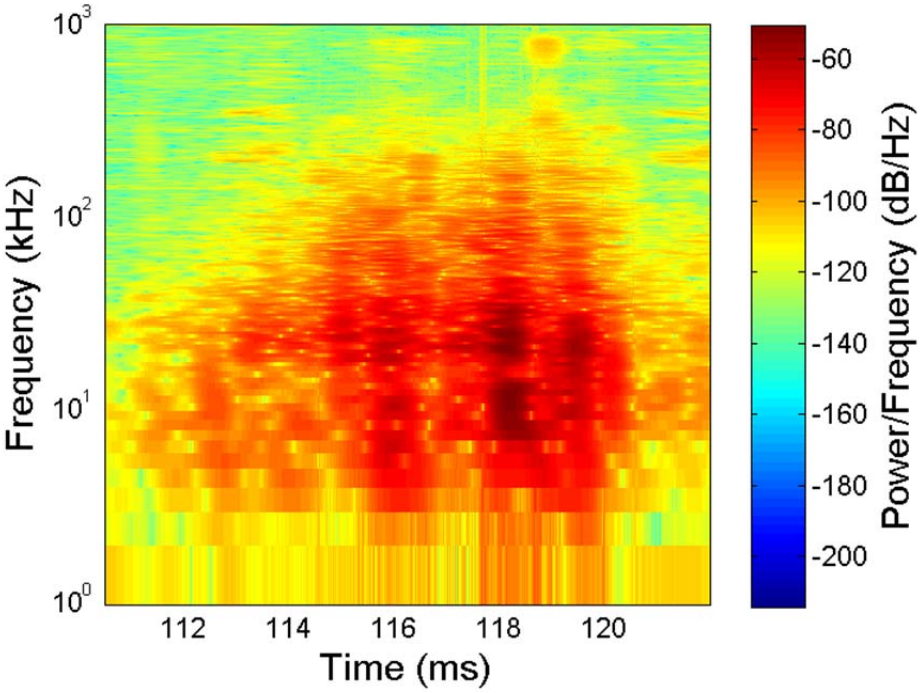

Figure 8. Spectrogram showing the power spectral density of a 2000 point (1ms) Hamming window in the acoustic emission in the failure test. The frequency with the most power, 24.5kHz, occurs at approximately 116 and 118ms. At the beginning of the time history, there is low frequency content from 3.9kHz to 52.7kHz followed by higher frequency content from 8.7kHz to 271.2kHz.

IV. DISCUSSION

This study provides a method of determining the location of an injury and demonstrates the efficacy of this method in a cervical spine. It develops the method using acoustic emissions generated at known locations using tap tests and applies this algorithm to the acoustic emission generated from a failure test in a whole cervical spine. The signals produced in the tap tests show small amplitude signals at the time the signal arrives at the sensors followed by larger signals. These small signals are approximately the same amplitude, which is expected

for a tap located 8mm from one sensor and 11mm from the other three. With a speed of sound of 3800m/s in bone [21], the wavelength for a 50kHz acoustic emission is 76mm. With such a large wavelength, it is not expected the signal amplitude would vary much over a relatively short difference in sensor distance. The larger signals following the smaller signal are most likely superposition of reflecting sound waves, and their amplitude is highly dependent on the position of the sensors and the path of the acoustic emission through the trabecular and cortical bone. The localization algorithm was able to determine the source of the acoustic emissions with an average error less than 4mm for the superior location and less than 11mm for the inferior location during calibration tests. This increased error is likely because the sound had to travel through one to four intervertebral discs before arriving at the sensor. There is a different effective speed of sound depending on how many discs the sound must traverse because intervertebral disc has a lower speed of sound than bone [22,23]. The algorithm assumes there is one effective speed of sound, which introduces error since the localization is performed using sensors placed on multiple vertebral bodies. The influence of this assumption can be reduced by using different speed of sounds for each sensor pair in the localization calculation. Experimentally, the effect of this assumption can be minimized by placing at least four sensors, the minimum number required to perform the calculation, on each vertebral body. Additional error is introduced because the algorithm assumes the load path is linear: the sound from the acoustic emission travels in a straight line to each sensor. The cervical spine has a complicated structure consisting of cortical bone, trabecular bone, ligaments and intervertebral discs, which may cause the sensor to acquire an initial acoustic signal that has propagated preferentially down a convoluted path driven by maximum speed of sound between emission source and the detecting sensor. Assuming the path is linear artificially increases the distance between the sensor and the acoustic emission source. The algorithm can be improved by using the structure known from the micro-CT to determine the possible load path and spatiotemporally constrain the problem.

The smallest distance this algorithm can resolve is 0.75mm based on an effective speed of sound of 1500m/s through whole spine and a sample frequency of 2MHz. Much of the error in the calculation is because the solution is sensitive to the selected time of arrivals. The localization methods used in homogeneous materials perform cross-correlations of the signals measured at the receivers to calculate the time of arrival. This method relies on the signal measured at each receiver to have only a time offset and amplitude differences, but have the same underlying frequency content. This technique is not applicable to spinal acoustic emission localization because of the complicated load path the sound takes before arriving at each sensor. Since the sound travels a different length and through different materials before arriving at each of the sensors, the resulting signal measured at each sensor can be drastically different in both amplitude and phase. In addition, multiple acoustic emissions can occur in close temporal proximity and the sensors are measuring the superposition and the reflection of these emissions, which can vary greatly depending on where the sensors are located. However, a reasonable assumption is that the first acoustic emission measured at each sensor location originated from the same location. The time of arrival of the first acoustic emission can be calculated automatically and with great repeatability by using the statistical approach of a standard deviation threshold used in this study.

The frequency response of the acoustic emission showed a wide band with a dominant frequency of 24.5kHz (Figure 7). The dominant frequency is in the range for ligament failure[17] and the peaks at 66.7kHz and 79.7kHz are in the expected range for bone failure [15,17,24,25]. These results agree with the CT and dissection showing osteophyte and ALL disruption. Variance in the frequency response of material failures in the spine are expected because bone, ligament and intervertebral disc have all been shown to be viscoelastic [26-30]. This viscoelasticity can cause attenuation of both the amplitude and the frequency of the signal causing the resulting response to be dependent on where it is measured relative to where the acoustic emission initially occurs. Also, the piezoelectric acoustic sensors used are more sensitive in the range from 110kHz to 2MHz than they are at frequencies outside this range. However, the frequency response of the acoustic emission during failure can be adjusted to account for this using the known frequency response of the sensor.

Additionally, the spectrogram (Figure 8) shows the content centered around 24.5kHz has substantial power at 116ms and 118ms, which is while the specimen is buckling. The high-speed video showed the osteophyte clearly dislodging from the C4 vertebral body at 118ms and anterior longitudinal ligament tearing. This frequency content is likely associated with the ALL failure from the large extension moment at the time the specimen buckles, or it may be associated with other soft tissue failure not observable on the micro-CT or in

dissection. The wide frequency band in both the power spectrum and the spectrogram suggest there is a distribution of soft tissue and hard tissue failure occurring simultaneously.

The algorithm was able to locate the source of an acoustic emission from a failure on an osteophyte with 12.2mm of error, which is adequate for determining the anatomical location that has failed. This error is inflated because the sensors were not placed in the ideal locations to perform the localization calculation. Without a priori knowledge of where the failure will occur, the best course of action is to place a minimum of four acoustic sensors on each vertebral body. This ensures that there is adequate instrumentation on each vertebral body to perform the localization.

The presented method is capable of localizing the first failure. If multiple failures occur simultaneously, the acoustic signal would show each of these individual acoustic emissions. If the failures occur in close temporal proximity, the signal may show the superposition of these individual failures. It would be very difficult to separate this signal out into its individual failures unless the signal consisted of failures of different materials. If ligamentous and bony failure occurred simultaneously, these signals could be band-pass filtered to show the acoustic signal of each material failure separately and the localization algorithm could be performed for each failure.

V. CONCLUSIONS

This study provides a methodology for assessing the failure location in a tissue model using a time difference of arrival algorithm. The presented data shows acoustic emissions can be localized in a cervical spine with a mean error as low as 3.63mm. Applying this same methodology to a failure test resulted in localization with 12.2mm error. This result can be improved by detailed assessment of acoustic paths between sensors. Additionally, a more refined model of the speed of sound along different ray paths is being investigated by leveraging the knowledge of the geometry of the specimen from the pre-test micro-CT scans. With further development, this algorithm should allow for even further localization of micro-failures, such as those in the trabeculae or in partial ligamentous tearing, which are likely associated with initiation of failure in impact biomechanics and repeated motion studies. Although only one specimen was tested, this study shows very good potential for using acoustic transducers to localize material failures in biological specimens. Traditional techniques rely on rapid drops in the force data or use the peak force to determine the ultimate strength. The failure in this study occurred while the cervical spine was buckling, which was prior to the peak force, indicating that injuries occurred that would not be accurately detected using traditional methods.

VI. ACKNOWLEDGEMENT

The authors would like to thank Naval Air Systems Command (NAVAIR) for providing funding and Augusto Alonso, Jason Luck, and Jason Kait for their assistance with the experimental setup.

VII. REFERENCES

[1] Côté P, Cassidy JD, Carroll L. The Saskatchewan Health and Back Pain Survey: The Prevalence of Neck Pain and Related Disability in Saskatchewan Adults. *Spine,* 1998, 23(15):1689-1698.

[2] Daffner SD, Hilibrand AS, Hanscom BS, Brislin BT, Vaccaro AR, Albert TJ. Impact of Neck and Arm Pain on Overall Health Status. *Spine,* 2003, 28(17):2030-2035.

[3] Côté P, Cassidy JD, Carroll L. The Treatment of Neck and Low Back Pain: Who Seeks Care? Who Goes Where? *Medical Care,* 2001, 39(9):956-967.

[4] Borghouts JAJ, Koes BW, Vondeling H, Bouter LM. Cost-of-illness of neck pain in The Netherlands in 1996. *Pain,* 1999, 80(3):629-636.

[5] Nightingale RW, McElhaney JH, Richardson WJ, Myers BS. Dynamic responses of the head and cervical spine to axial impact loading. *Journal of Biomechanics,* 1996, 29(3):307-318.

[6] Van Ee CA, Nightingale RW, Camacho DL, et al. Tensile properties of the human muscular and ligamentous cervical spine. *Stapp car crash journal,* 2000, 44:85-102.

[7] Nightingale RW, McElhaney JH, Camacho DL, Kleinberger M, Winkelstein BA, Myers BS. *The dynamic responses of the cervical spine: buckling, end conditions, and tolerance in compressive impacts.* SAE Technical Paper;1997.

[8] Yoganandan N, Kumaresan S, Pintar FA. Geometric and Mechanical Properties of Human Cervical Spine Ligaments. *Journal of Biomechanical Engineering,* 2000, 122(6):623-629.
[9] Bass CR, Lucas SR, Salzar RS, et al. Failure Properties of Cervical Spinal Ligaments Under Fast Strain Rate Deformations. *Spine,* 2007, 32(1):E7-E13.
[10] Gunning JL, Callaghan JP, McGill SM. Spinal posture and prior loading history modulate compressive strength and type of failure in the spine: a biomechanical study using a porcine cervical spine model. *Clinical Biomechanics,* 2001, 16(6):471-480.
[11] Pintar FA, Yoganandan N, Myers T, Elhagediab A, Sances A. Biomechanical properties of human lumbar spine ligaments. *Journal of biomechanics,* 1992, 25(11):1351-1356.
[12] Mosekilde L. Age-related changes in vertebral trabecular bone architecture—assessed by a new method. *Bone,* 1988, 9(4):247-250.
[13] Grosse C, Reinhardt H, Finck F. Signal-Based Acoustic Emission Techniques in Civil Engineering. *Journal of Materials in Civil Engineering,* 2003, 15(3):274-279.
[14] Allsop DL, Perl TR, Warner CY. Force-Deflection and Fracture Characteristics of the Temporo-Parietal Region of the Human Head. *Training,* 1991, 2007:07-17.
[15] Funk JR, Khaewpong N, Eppinger RH, et al. The Axial Injury Tolerance of the Human Foot/Ankle Complex and the Effect of Achilles Tension. *Journal of Biomechanical Engineering,* 2002, 124(6):750-757.
[16] Schmidt AL, Paskoff G, Shender BS, Bass CR. Risk of Lumbar Spine Injury From Cyclic Compressive Loading. *Spine,* 2012, 37(26):E1614-E1621.
[17] Van Toen C, Street J, Oxland TR, Cripton PA. Acoustic emission signals can discriminate between compressive bone fractures and tensile ligament injuries in the spine during dynamic loading. *Journal of Biomechanics,* 2012, 45(9):1643-1649.
[18] Carpinteri A, Lacidogna G, Niccolini G. Critical behaviour in concrete structures and damage localization by acoustic emission. *Key Engineering Materials,* 2006, 312:305-310.
[19] Leone C, Lopresto V, Papa I, Caprino G. Triangulation method as a valid tool to locate the damage in unidirectional CFRP laminates. *Composite Structures,* 2012, 94(8):2418-2423.
[20] Berkovits A, Fang D. Study of fatigue crack characteristics by acoustic emission. *Engineering Fracture Mechanics,* 1995, 51(3):401-416.
[21] Vega E, Wittich A, Mautalen C, Carrilero P, Sahores AO, Silberman F. Tibial Ultrasound Velocity in Normal and Hip Fracture Women. *Journal of Clinical Densitometry,* 1998, 1(2):179-185.
[22] Lochmüller EM, Eckstein F, Kaiser D, et al. Prediction of vertebral failure loads from spinal and femoral dual-energy x-ray absorptiometry, and calcaneal ultrasound: an in situ analysis with intact soft tissues. *Bone,* 1998, 23(5):417-424.
[23] Rossman P, Zagzebski J, Mesina C, Sorenson J, Mazess R. Comparison of speed of sound and ultrasound attenuation in the os calcis to bone density of the radius, femur and lumbar spine. *Clinical Physics and Physiological Measurement,* 1989, 10(4):353.
[24] Sugiyama H, Whiteside LA, Kaiser AD. Examination of Rotational Fixation of the Femoral Component in Total Hip Arthroplasty: A Mechanical Study of Micromovement and Acoustic Emission. *Clinical Orthopaedics and Related Research,* 1989, 249:122-128.
[25] Schwalbe H-J, Bamfaste G, Franke R-P. Non-destructive and non-invasive observation of friction and wear of human joints and of fracture initiation by acoustic emission. *Proceedings of the Institution of Mechanical Engineers, Part H: Journal of Engineering in Medicine,* 1999, 213(1):41-48.
[26] McElhaney JH. Dynamic response of bone and muscle tissue. *Journal of Applied Physiology,* 1966, 21(4):1231-1236.
[27] Lucas SR, Bass CR, Salzar RS, et al. Viscoelastic properties of the cervical spinal ligaments under fast strain-rate deformations. *Acta Biomaterialia,* 2008, 4(1):117-125.
[28] Myers BS, McElhaney JH, Doherty BJ. The viscoelastic responses of the human cervical spine in torsion: Experimental limitations of quasi-linear theory, and a method for reducing these effects. *Journal of Biomechanics,* 1991, 24(9):811-817.
[29] Guilak F, Ting-Beall HP, Baer AE, Trickey WR, Erickson GR, Setton LA. Viscoelastic Properties of Intervertebral Disc Cells: Identification of Two Biomechanically Distinct Cell Populations. *Spine,* 1999, 24(23):2475.
[30] Leahy JC, Hukins DWL. Viscoelastic properties of the nucleus pulposus of the intervertebral disk in compression. *Journal of Materials Science: Materials in Medicine,* 2001, 12(8):689-692.